PROCEEDINGS OF SCIENCE

Feasibility study on an analysis of CR helium flux with the CALET detector based on an extended acceptance

M. Mattiazzi[a,b,*] **and P. Brogi**[a,c] **for the CALET collaboration**

[a]*Department of Physical Sciences, Earth and Environment, University of Siena,*
via Roma 56, 53100 Siena, Italy

[b]*INFN Sezione di Padova,*
Via Marzolo, 8, 35131 Padova, Italy

[c]*INFN Sezione di Pisa,*
Polo Fibonacci, Largo B. Pontecorvo, 3, 56127 Pisa, Italy

E-mail: marco.mattiazzi@pd.infn.it

In this work, we present a feasibility study aiming at an enhanced statistical precision of CR helium flux with CALET data. It is based on a wider acceptance with respect to the present fiducial one while ensuring a correct identification of charged particles crossing the detector within much wider geometrical configurations. The expected statistical enhancement for the all-acceptance configuration is nearly 2× with respect to the previous analysis, over the entire energy range (from tens of GeV, up to hundreds of TeV). Preliminary assessment of efficiencies and background sources has been carried out based on energy-dependent charge selections.

38th International Cosmic Ray Conference (ICRC2023)
26 July - 3 August, 2023
Nagoya, Japan

*Speaker

1. Introduction

The CALorimetric Electron Telescope (CALET) is a space-based experiment operating on-board the International Space Station (ISS) since August 2015 and taking data smoothly since mid-October 2015.

It is composed of three sub-systems for cosmic ray detection. At the top of the instrument is the CHarge Detector (CHD), a two-layer hodoscope segmented into 14 plastic scintillator paddles, with dimensions 32 mm (W) $\times$ 10 mm (H) $\times$ 450 mm (L). The two arrays of paddles are oriented perpendicularly, providing an independent charge measurement of the impinging particle for each view. Beneath the CHD, is the calorimeter with a total thickness of 30 X_0 and in turn divided into two sub-detectors. In the upper part, the IMaging Calorimeter (IMC) is a fine-grained pre-shower sampling calorimeter with a thickness of 3 X_0, enabling independent charge assessment through multiple dE/dx samplings. It consists of 7 layers of tungsten plates, each separated by two alternate layers of square scintillating fibers with cross section 1 mm^2 and 448 mm long. The particle showers are sampled every 0.2 X_0 by the first 5 layers, whereas the last two layers provide 1.0 X_0 sampling. At the bottom of the instrument is the Total AbSorption Calorimeter (TASC), an homogeneous calorimeter with a thickness of 27 X_0. It consists of 12 layers, each composed of an array of 16 lead-tungstate (PWO) logs with dimensions 19 mm (W) $\times$ 20 mm (H) $\times$ 450 mm (L). These are aligned in pairs along the directions *x* - *y* and permit the reconstruction of the shower profile, discriminating its electromagnetic or hadronic nature with high rejection power. The helium flux measurement with CALET has been recently published in [3], covering a wide energy range from $\sim$ 40 GeV to $\sim$ 250 TeV. The measured spectrum confirms the deviation of the flux from a single power law. A progressive spectral hardening from a few hundred GeV to a few tens of TeV and the onset of a softening around 30 TeV has been observed. At higher energies, a limiting factor to better resolve the spectral features is the statistics. In this work we present a feasibility study aiming at an enhanced statistical precision of CR helium flux with CALET data at high energies. It is based on a wider acceptance with respect to the present fiducial acceptance A_1 [3] while ensuring a correct identification of helium nuclei crossing the detector.

2. Acceptance categories
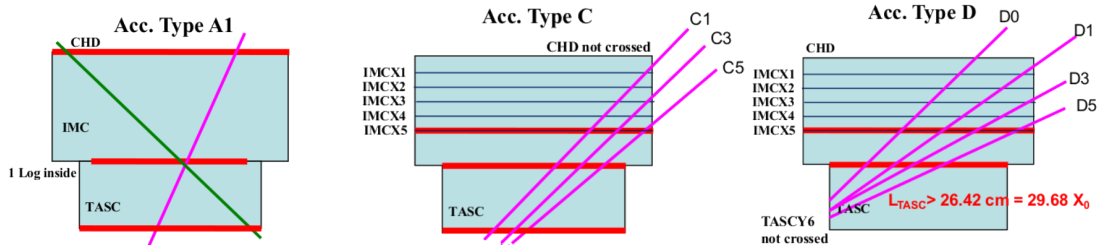
Figure 1: Definition of geometric configurations. Type A_1 is used in current helium analysis [3].

The acceptance A_1 and the additional geometric configurations studied in this work are illustrated in fig. 1. In detail, the reconstructed track must cross for: $\mathbf{A_1}$, the entire detector, from the top of the CHD to the bottom of the TASC, with a 2 cm margin from the edge of the TASC first layer;

C_i, the entire TASC and the IMC detector starting from the i-th layer; D_i, the IMC detector starting from the i-th layer and at least 27 cm (equivalent to $\sim 30X_0$) of TASC detector to ensure a reliable energy determination. In the D_0 acceptance, the incoming particle must pass also the entire CHD.

3. Selection criteria

3.1 Pre-selection

The first step of the analysis procedure is based on a set of common criteria for the selection of a well-reconstructed sample of events, both for the A1 and the other geometric configurations. Such event selections are optimized using MC simulations based on the EPICS simulation package [7], which allows to reproduce both the detector configuration and response, based on the physical processes involved. Pre-selection is realized by applying the following cuts :

Off-line trigger validation relies on more stringent thresholds than the on-line trigger for suppressing variations of detector gains;

Track quality cut ensures an high-quality track selection using performance metrics derived from the application of combinatorial KF tracking algorithm [1];

Geometric requirements holds as the reconstructed track crosses the fiducial volume defined by the configuration being analyzed;
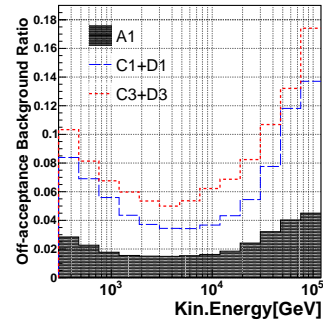
Electron rejection cut is based on fix-thresholds on an empirical Moliere concentration and on the fraction of energy deposited in the last layer of the TASC.

More details about such a data reduction can be found in [2, 3].

3.2 Off-acceptance rejection based on Boosted Decision Tree

For geometrical conditions other than A_1, a progressive enhancement of the off-acceptance background is observed with increasing inclination of the track. This is mainly due to the partial degradation of the tracking performance, resulting from the limited shower development in the TASC for inclined tracks. Therefore, for events crossing the TASC detector laterally, it is more probable that a secondary being mislabeled as primary particle, increasing the off-acceptance background. Just by acceptance $C_1 + D_1$, out-of-acceptance background grows to more than double comparing to the same component in configuration A_1, as it can be appreciated from fig. 2.

Figure 2: Off-acceptance background component for acceptances A_1, $C_1 + D_1$ and $C_3 + D_3$ applying standard selections.

A machine learning approach, based on Boosted Decision Tree (BDT), has been tested, aiming to improve the rejection of such background. This has the benefit of making tailored selections related to the reconstructed event topology. As a result of preliminary studies based on background rejection power and best tuned FD-MC distributions, the input features that have been considered, are:

3

- Energy deposition profile, based on the fraction of energy deposited on each TASC layers. All layers, except the 2nd ,3rd and 4th , have been used.

- Topological variables built from the difference between the track reconstructed with combinatorial Kalman filter and with the method of moments [4]. The former mainly exploits the information provided by the IMC sub-system, whereas the latter leverages on TASC segmentation. In detail, Δ_{TK}^{X} (Δ_{TK}^{Y}) defined as the difference between position in X (Y) coordinates of the impact point on first TASC layer, and Θ_{TK}^{X} (Θ_{TK}^{Y}), defined as the difference between the reconstructed angle of the tracks in X (Y) views, have been selected.

Next, BDT classifiers have been evaluated in 6 large bins of deposited energy[1] for the configurations $A_1 + D_0$, $C_1 + D_1$, $C_2 + D_2$ and $C_3 + D_3$. The reliability of BDT model has been assessed by randomly dividing MC data into training and testing samples to check the agreement of signal and background classifier distributions. To set BDT working point, the maximum of significance has been estimated for each energy bin. Some results for the energy bin $6.5\,\text{TeV} < E_{dep}^{TASC} < 20\,\text{TeV}$ are illustrated in fig. 3.
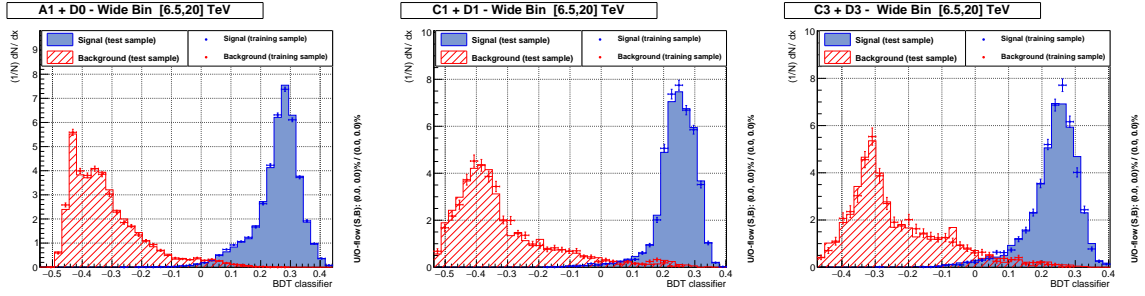
Figure 3: BDT model performance evaluated splitting randomly the MC data in test and training samples, for the configurations $A_1 + D_0$, $C_1 + D_1$ and $C_3 + D_3$ in the energy bin $6.5\,\text{TeV} < E_{dep}^{TASC} < 20\,\text{TeV}$.

3.3 Charge identification

In helium analysis charge identification is of paramount importance to achieve a reliable proton rejection over the entire energy range. Energy-dependent charge selections have been carried out for each combined acceptance, with a procedure analogous to that applied in [3].

Proton and helium charge distributions from FD and MC samples are fitted with the convolution of a Landau with a Gaussian distribution. Peak position μ , the LHWHM σ_L and the RHWHM σ_R, defined as $\sigma_R + \sigma_L = $ FWHM, are extracted for each energy bin. Then, the same quantities are interpolated with high-order logarithmic polynomials[2] such that they are continuously defined for each energy deposited.

As shown in fig. 4, helium charge distributions get broader as energy and track tilt increase. Hence, for this analysis helium events are selected according to

---

[1]In detail, `TMVA` package [5] has been used, and the energy intervals in E_{dep}^{TASC} are: < 30 GeV, [30 , 120] GeV, [120 , 300] GeV, [300 GeV, 6.5 TeV], [6.5 , 20] TeV, > 20 TeV.

[2]defined as $p_n(E) = \sum_{i=0}^{n} c_i \log(E)^i$. A third order log-polynomials were chosen for this analysis.

4

$$\mu_{He}(E) - n_L \sigma_L(E) \; < \; Z \; < \; \mu_{He}(E) + n_R \sigma_R(E)$$

where n_R is fixed at 5 over the entire energy range, whereas n_R is initially set to 3 and then it is lowered to 2 in the region of higher energies, taking into account the broadening of the charge distribution with respect to the number of IMC layers crossed by the track and for the track tilt angle, as shown in fig. 4. This approach allows a nearly flat charge selection efficiency above 500 GeV, while containing the rise of proton contamination.
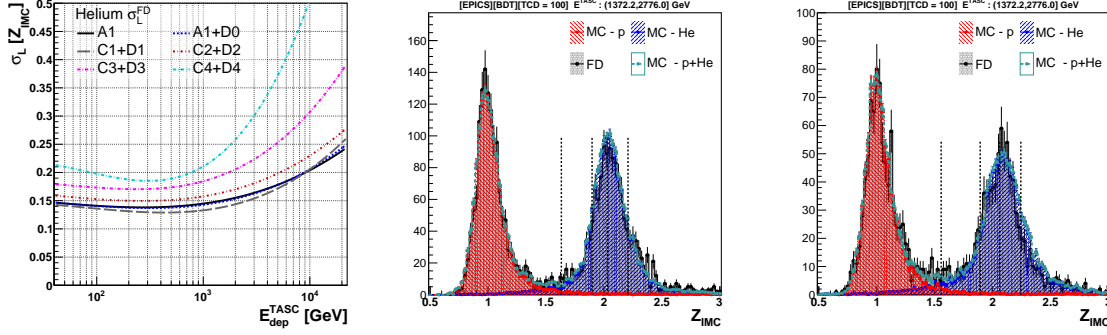
Figure 4: (Left) σ_L for FD data as function of TASC deposited energy for acceptances A_1, A_1+D_0, and C_i+D_i (Right) Charge distributions for acceptances C_1+D_1 and C_2+D_2 in the energy bin $1.4\,\text{TeV} < E_{dep}^{TASC} < 2.8\,\text{TeV}$. The distributions from MC proton and helium samples are superimposed to FD data.

Further extensions to highly tilted events (acceptances $C_4 + D_4$ and $C_5 + D_5$) require additional work and are not including in this paper.

4. Feasibility studies on extended acceptance configurations

In order to enhance the statistical precision of CR helium flux with CALET data, the extended acceptances $K_m := A_1 + D_0 + \sum_{i=1}^{m}(C_i + D_i)$ have been defined where only the IMC provides for charge identification. The statistical gain that can be estimated from the geometrical factor is summarized in table 1.

Acceptance Type	Geometric Factor [cm^2 sr]	Statistical Gain (normalized to A1)
A1	510	1
K1 := A1+D0 + (C1+D1)	688	1.35
K3 := K2 + (C3+D3)	819.6	1.6

Table 1: Geometric factors and the related statistical gain for K_1 and K_3 extended acceptance types.

4.1 Energy range

The energy range, whereto an increase of the acceptance is beneficial, has been estimated by computing the purity estimator. It is defined as the ratio of selected helium nuclei after the background subtraction (signal) divided by the total number of events reconstructed as helium

(signal + background[3]). As shown in fig. 5, purity analysis indicates that it is reasonable to include events with larger inclination, only for energies greater than 500 GeV where similar or even better values are achieved compared with the standard analysis. The improved performance at high energies can be attributed to the new BDT-based analysis strategy. In contrast, the worse performance at low energies is due to the absence of the CHD sub-system for charge identification, resulting in an increased proton contamination.
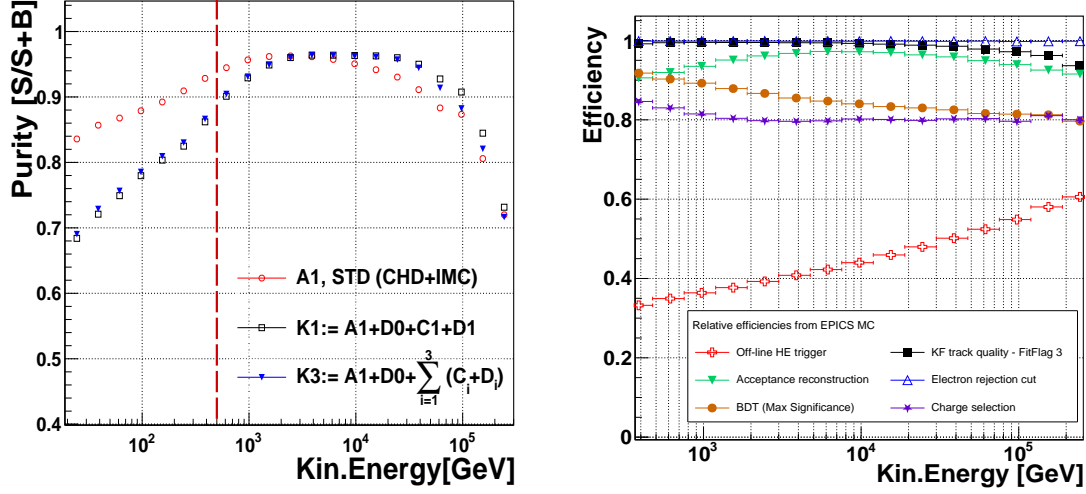
Figure 5: (Left) Purity quantity as function of kinetic energy for acceptance A_1 with standard selections, and K_1, K_3 with BDT-based off-acceptance cuts. The red dashed line is set at 500 GeV kinetic energy. (Right) Efficiencies of K_3 configuration for each selection step as function of kinetic energy.

4.2 Efficiencies and effective acceptance

For each selection stage, efficiency was calculated as the ratio of events passing the current stage to those passing all the previous ones. The results, for K_3 configuration, are illustrated in the right-hand panel of fig. 5. The results are compatible with the ones in fiducial acceptance for kinetic energies greater than 500 GeV. The effective acceptance[4] for configuration A_1, K_1 and K_3 are shown in fig. 6. A statistical gain up to $\sim 60\%$ is achieved for K_3 configuration with respect to A_1.

4.3 Stability test of unfolding procedure

Extending the geometric acceptance to more inclined tracks could impact the energy resolution for hadronic showers and therefore the unfolding procedure. Another key test to assess the feasibility of extending the geometric acceptance, is to verify the stability of the Bayesian unfolding procedure[5] for inferring the primary energy of the incoming particle from the fraction of energy deposited on TASC [2]. The pull test has been selected for such validation.

---

[3]Background assessment and subtraction has been performed with the same procedure of A_1 analysis [3].

[4]defined as the total efficiency multiplied by the geometric factor

[5]performed with `ROOUnfold` package [6], using two iterations due to the accuracy of the prior distribution
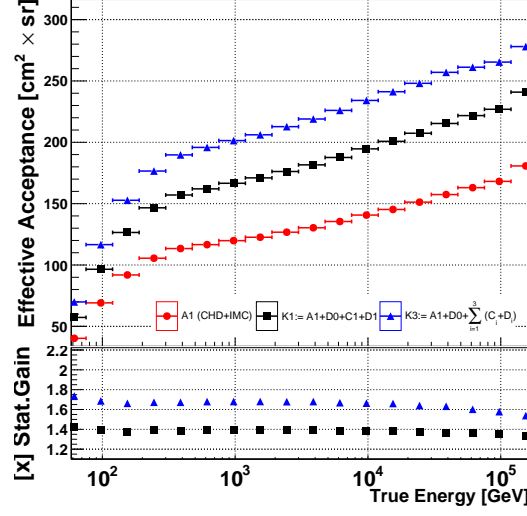
Figure 6: Effective acceptance for A_1, K_1 and K_3, after all the selections, and, in the lower panel, the statistical gain normalized to A_1.

Each helium MC event from the real acceptance K_3, which satisfies all the selections criteria, is fluctuated according to the Poisson statistics with a mean of one. This procedure is repeated N_{toy} times, resulting in[6] $\{n_{DEP}^{TOY,i}\}_{i=1,\cdots,N_{toy}}$ newly sampled histograms as a function of the deposited energy. Each of these histograms is then unfolded with the response matrix derived from no fluctuations in the MC sample, getting $\{n_{UNFLD}^{TOY,i}\}_{i=1,\cdots,N_{toy}}$. The pull distribution is then computed bin-by-bin as the difference between $n_{UNFLD}^{TOY,i}$ spectrum and the unfolded histogram derived without re-sampling n_{UNFLD}^0, divided by the statistical uncertainty σ_{UNFLD}^0 provided by the unfolding routine in the latter case.
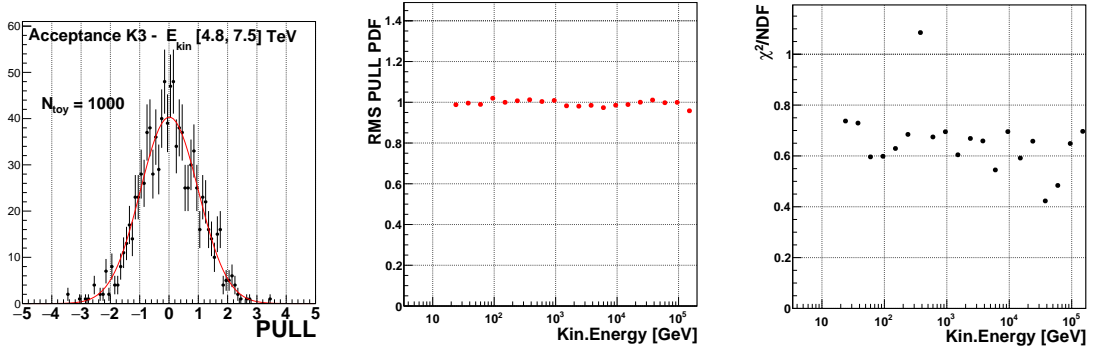
Figure 7: (Right) Pull distribution for energy bin 4.8 TeV < E_{dep}^{TASC} < 7.5TeV (Middle) RMS and (Right) χ^2/NDF for Gaussian fit of pull distribution for each energy bin of the spectrum.

For each energy bin, the pull distributions shows that iterative bayesian unfolding procedure from EPICS MC in K_3 geometric configuration, is stable because the distributions from the pseudo-

---

[6]where n_{DEP} stands for $\frac{dN}{dE_{DEP}}$

experiments can be fitted with a Gaussian curve to very high degree of accuracy (χ^2/NDF ~ 1). The statistical uncertainties are estimated properly as well, since the RMS ~ 1 in the entire energy range. The results are shown in fig. 7.

5. Conclusions

In our current helium analysis [3], approximately 50% of the total geometric factor is used to obtain the flux. Less stringent geometric requirements, while performing the same selections, lead to both a progressive increase in off-acceptance events and an overall rise in proton contamination, caused by the partial degradation of tracking performance for very inclined primaries, and the lack of the CHD sub-system for charge identification.

In this work, the possibility of mitigating these issues has been investigated by introducing a BDT-based off-acceptance background rejection and an energy-dependent charge selection, both tailored to the topology of the event in extended acceptance.

The results indicate that extending the helium flux measurement to K_3 acceptance is feasible above 500 GeV in kinetic energy, with a statistical gain up to $\sim 60\%$.

References

[1] P. Maestro and N. Mori (for the CALET Collab.), PoS (ICRC2017) 208 (2017).

[2] P. Brogi et al. , PoS (ICRC2021) 101 (2021)

[3] O. Adriani et al. (CALET Collab.), Phys. Rev. Lett. **130**, 171002 (2023).

[4] J. J. Gomez et al., Nucl. Instr. Meth. Phys. Res. A, 262(2-3), 284–290, 1987.

[5] A. Hoecker, et al. "TMVA: Toolkit for Multivariate Data Analysis," PoS A CAT 040 (2007) [physics/0703039].

[6] Brenner et al., "Comparison of unfolding methods using RooFitUnfold." International Journal of Modern Physics A (2019)

[7] K. Kasahara, Proc. 24th Intl. Cosmic Ray Conf., Rome, Italy, ed. by N. Iucci and E. Lamanna (Intl. Union of Pure and Applied Phys. 1, 399 (1995)

Full Author List: CALET Collaboration

O. Adriani[1,2], Y. Akaike[3,4], K. Asano[5], Y. Asaoka[5], E. Berti[2,6], G. Bigongiari[7,8], W.R. Binns[9], M. Bongi[1,2], P. Brogi[7,8], A. Bruno[10], N. Cannady[11,12,13], G. Castellini[6], C. Checchia[7,8], M.L. Cherry[14], G. Collazuol[15,16], G.A. de Nolfo[10], K. Ebisawa[17], A.W. Ficklin[14], H. Fuke[17], S. Gonzi[1,2,6], T.G. Guzik[14], T. Hams[11], K. Hibino[18], M. Ichimura[19], K. Ioka[20], W. Ishizaki[5], M.H. Israel[9], K. Kasahara[21], J. Kataoka[22], R. Kataoka[23], Y. Katayose[24], C. Kato[25], N. Kawanaka[20], Y. Kawakubo[14], K. Kobayashi[3,4], K. Kohri[26], H.S. Krawczynski[9], J.F. Krizmanic[12], P. Maestro[7,8], P.S. Marrocchesi[7,8], A.M. Messineo[8,27], J.W. Mitchell[12], S. Miyake[28], A.A. Moiseev[29,12,13], M. Mori[30], N. Mori[2], H.M. Motz[31], K. Munakata[25], S. Nakahira[17], J. Nishimura[17], S. Okuno[18], J.F. Ormes[32], S. Ozawa[33], L. Pacini[2,6], P. Papini[2], B.F. Rauch[9], S.B. Ricciarini[2,6], K. Sakai[11,12,13], T. Sakamoto[34], M. Sasaki[29,12,13], Y. Shimizu[18], A. Shiomi[35], P. Spillantini[1], F. Stolzi[7,8], S. Sugita[34], A. Sulaj[7,8], M. Takita[5], T. Tamura[18], T. Terasawa[5], S. Torii[3], Y. Tsunesada[36,37], Y. Uchihori[38], E. Vannuccini[2], J.P. Wefel[14], K. Yamaoka[39], S. Yanagita[40], A. Yoshida[34], K. Yoshida[21], and W.V. Zober[9]

[1]Department of Physics, University of Florence, Via Sansone, 1 - 50019, Sesto Fiorentino, Italy, [2]INFN Sezione di Firenze, Via Sansone, 1 - 50019, Sesto Fiorentino, Italy, [3]Waseda Research Institute for Science and Engineering, Waseda University, 17 Kikuicho, Shinjuku, Tokyo 162-0044, Japan, [4]JEM Utilization Center, Human Spaceflight Technology Directorate, Japan Aerospace Exploration Agency, 2-1-1 Sengen, Tsukuba, Ibaraki 305-8505, Japan, [5]Institute for Cosmic Ray Research, The University of Tokyo, 5-1-5 Kashiwa-no-Ha, Kashiwa, Chiba 277-8582, Japan, [6]Institute of Applied Physics (IFAC), National Research Council (CNR), Via Madonna del Piano, 10, 50019, Sesto Fiorentino, Italy, [7]Department of Physical Sciences, Earth and Environment, University of Siena, via Roma 56, 53100 Siena, Italy, [8]INFN Sezione di Pisa, Polo Fibonacci, Largo B. Pontecorvo, 3 - 56127 Pisa, Italy, [9]Department of Physics and McDonnell Center for the Space Sciences, Washington University, One Brookings Drive, St. Louis, Missouri 63130-4899, USA, [10]Heliospheric Physics Laboratory, NASA/GSFC, Greenbelt, Maryland 20771, USA, [11]Center for Space Sciences and Technology, University of Maryland, Baltimore County, 1000 Hilltop Circle, Baltimore, Maryland 21250, USA, [12]Astroparticle Physics Laboratory, NASA/GSFC, Greenbelt, Maryland 20771, USA, [13]Center for Research and Exploration in Space Sciences and Technology, NASA/GSFC, Greenbelt, Maryland 20771, USA, [14]Department of Physics and Astronomy, Louisiana State University, 202 Nicholson Hall, Baton Rouge, Louisiana 70803, USA, [15]Department of Physics and Astronomy, University of Padova, Via Marzolo, 8, 35131 Padova, Italy, [16]INFN Sezione di Padova, Via Marzolo, 8, 35131 Padova, Italy, [17]Institute of Space and Astronautical Science, Japan Aerospace Exploration Agency, 3-1-1 Yoshinodai, Chuo, Sagamihara, Kanagawa 252-5210, Japan, [18]Kanagawa University, 3-27-1 Rokkakubashi, Kanagawa, Yokohama, Kanagawa 221-8686, Japan, [19]Faculty of Science and Technology, Graduate School of Science and Technology, Hirosaki University, 3, Bunkyo, Hirosaki, Aomori 036-8561, Japan, [20]Yukawa Institute for Theoretical Physics, Kyoto University, Kitashirakawa Oiwake-cho, Sakyo-ku, Kyoto, 606-8502, Japan, [21]Department of Electronic Information Systems, Shibaura Institute of Technology, 307 Fukasaku, Minuma, Saitama 337-8570, Japan, [22]School of Advanced Science and Engineering, Waseda University, 3-4-1 Okubo, Shinjuku, Tokyo 169-8555, Japan, [23]National Institute of Polar Research, 10-3, Midori-cho, Tachikawa, Tokyo 190-8518, Japan, [24]Faculty of Engineering, Division of Intelligent Systems Engineering, Yokohama National University, 79-5 Tokiwadai, Hodogaya, Yokohama 240-8501, Japan, [25]Faculty of Science, Shinshu University, 3-1-1 Asahi, Matsumoto, Nagano 390-8621, Japan, [26]Institute of Particle and Nuclear Studies, High Energy Accelerator Research Organization, 1-1 Oho, Tsukuba, Ibaraki, 305-0801, Japan, [27]University of Pisa, Polo Fibonacci, Largo B. Pontecorvo, 3 - 56127 Pisa, Italy, [28]Department of Electrical and Electronic Systems Engineering, National Institute of Technology (KOSEN), Ibaraki College, 866 Nakane, Hitachinaka, Ibaraki 312-8508, Japan, [29]Department of Astronomy, University of Maryland, College Park, Maryland 20742, USA, [30]Department of Physical Sciences, College of Science and Engineering, Ritsumeikan University, Shiga 525-8577, Japan, [31]Faculty of Science and Engineering, Global Center for Science and Engineering, Waseda University, 3-4-1 Okubo, Shinjuku, Tokyo 169-8555, Japan, [32]Department of Physics and Astronomy, University of Denver, Physics Building, Room 211, 2112 East Wesley Avenue, Denver, Colorado 80208-6900, USA, [33]Quantum ICT Advanced Development Center, National Institute of Information and Communications Technology, 4-2-1 Nukui-Kitamachi, Koganei, Tokyo 184-8795, Japan, [34]College of Science and Engineering, Department of Physics and Mathematics, Aoyama Gakuin University, 5-10-1 Fuchinobe, Chuo, Sagamihara, Kanagawa 252-5258, Japan, [35]College of Industrial Technology, Nihon University, 1-2-1 Izumi, Narashino, Chiba 275-8575, Japan, [36]Graduate School of Science, Osaka Metropolitan University, Sugimoto, Sumiyoshi, Osaka 558-8585, Japan, [37]Nambu Yoichiro Institute for Theoretical and Experimental Physics, Osaka Metropolitan University, Sugimoto, Sumiyoshi, Osaka 558-8585, Japan, [38]National Institutes for Quantum and Radiation Science and Technology, 4-9-1 Anagawa, Inage, Chiba 263-8555, Japan, [39]Nagoya University, Furo, Chikusa, Nagoya 464-8601, Japan, [40]College of Science, Ibaraki University, 2-1-1 Bunkyo, Mito, Ibaraki 310-8512, Japan